Bissantz, Nicolai; Holzmann, Hajo; Pawlak, Mirosław

Working Paper

Testing for image symmetries: with application to confocal microscopy

Technical Report, No. 2008,18

Provided in Cooperation with:
Collaborative Research Center 'Reduction of Complexity in Multivariate Data Structures' (SFB 475), University of Dortmund

Suggested Citation: Bissantz, Nicolai; Holzmann, Hajo; Pawlak, Mirosław (2008) : Testing for image symmetries: with application to confocal microscopy, Technical Report, No. 2008,18, Technische Universität Dortmund, Sonderforschungsbereich 475 - Komplexitätsreduktion in Multivariaten Datenstrukturen, Dortmund

This Version is available at:
https://hdl.handle.net/10419/36592

Testing for Image Symmetries – with Application to Confocal Microscopy

Nicolai Bissantz[1] , Hajo Holzmann[2,3], and Mirosław Pawlak[4]

[1]Fakultät für Mathematik
Ruhr-Universität Bochum, Germany

[2]Institut für Stochastik
Karlsruhe University, Germany,

and

[4]Department of Electrical and Computer Engineering,
The University of Manitoba, Winnipeg, Canada

July 11, 2008

Abstract

Statistical tests are introduced for checking whether an image function $f(x, y)$ defined on the unit disc $D = \{(x, y) : x^2 + y^2 \leq 1\}$ is invariant under certain symmetry transformations of D, given that discrete and noisy data are observed. We consider invariance under reflections or under rotations by rational angles, as well as joint invariance under both reflections and rotations. Furthermore, we propose a test for rotational invariance of $f(x, y)$, i.e., for checking whether $f(x, y)$, after transformation to polar coordinates, only depends on the radius and not on the angle. These symmetry relations can be naturally expressed as restrictions for the Zernike moments of the image function $f(x, y)$, i.e., the Fourier coefficients with respect to the Zernike orthogonal basis. Therefore, our test statistics are based on checking whether the estimated Zernike coefficients approximately satisfy those restrictions. This is carried out by forming the L_2 distance between the image function and its transformed version obtained by some symmetry transformation. We derive the asymptotic distribution of the test statistics under both the hypothesis of symmetry as well as under fixed alternatives. Furthermore, we investigate the quality of the asymptotic approximations via simulation studies. The usefulness our theory is verified by examining an important problem in confocal microscopy, i.e., we investigate possible imprecise alignments in the optical path of the microscope. For optical systems with rotational symmetry, the theoretical point-spread-function (PSF) is reflection symmetric with respect to two orthogonal axes, and rotationally invariant if the detector plane matches the optical plane of the microscope. We use our tests to investigate whether the required symmetries can indeed be detected in the empirical PSF.

Index Terms: image symmetry, symmetry detection, nonparametric estimation, Zernike moments, nanoscale bioimaging, point-spread-function

[3]Corresponding author: Dr. Hajo Holzmann, Institut für Stochastik, Karlsruhe University, Englerstr. 2, D-76128 Karlsruhe, Germany, email: holzmann@stoch.uni-karlsruhe.de, Fon: +49 721 608 3272 Fax: +49 721 608 6066

1 Introduction

Symmetry has been thoroughly studied in art, science, and the real world for a long time [40, 9]. This fundamental concept has been described and analysed using various mathematical tools aiming in characterizing the symmetries of objects. Symmetry also plays an important role in image analysis and understanding and finds direct applications in object recognition, robotics, image animation, and image compression. Of particular interest is how to test the hypothesis of basic types of symmetry present in an object based on its discrete and noisy observations. This paper formulates the statistical problem of detecting image symmetry for two-dimensional objects, and develops corresponding rigorous statistical testing procedures. Furthermore, we apply our symmetry detection methods to a problem arising in confocal microscopy. From the optical properties of the microscope, the so-called point-spread function (PSF) can be computed and it is characterized by certain symmetry relations such as reflection symmetry with respect to two orthogonal axes. The PSF may even reveal rotational symmetry if the optical system is rotationally symmetric and the detector plane matches the optical plane of the microscope. A precise knowledge of the PSF is essential in image recovery since the observed image is obtained by convolution of the underlying object with the PSF. Due to, however, imprecise alignment of elements in the optical path of the microscope, the actual PSF may possible be asymmetric, and therefore there is a need for detecting symmetries in the observed PSF.

With this practical motivation in mind let us consider some basic symmetry concepts for two-dimensional objects. Symmetry in two dimensions can be defined in terms of a combination of two geometric transformations, namely reflection and rotation. In fact, a finite non-periodic two-dimensional object may exhibit only these two kinds of symmetries, see [9] for a full account of the problem of classification and enumeration of symmetric patterns. Hence, a planar object is said to be symmetric (with respect to the aforementioned transformations) if its transformed version is the same as the original form. In particular, an image shows rotational symmetry of order $d \geq 2$ (d being an integer) if it is invariant under rotations through an angle $2\pi/d$ and its integer multiples about the centre of mass of the object. The case $d = 2$ corresponds to the requirement that $r_2 f(x, y) = f(x, y)$, where $r_2 f(x, y) = f(-x, -y)$ is the image rotation through an angle π. Yet another important case of rotational symmetry is when $d = \infty$, i.e., we have circular symmetric image $f(x, y) = g(\sqrt{x^2 + y^2})$, for some univariate function $g(\cdot)$. On the other hand, an image reveals reflectional symmetry if it is invariant to reflection with respect to one or more lines called axes of symmetry. If there is only one axis of symmetry and it aligns with the $y-$axis, the reflectional symmetry is defined as follows $\tau f(x, y) = f(x, y)$, where $\tau f(x, y) = f(-x, y)$.

The problem of detecting and measuring object symmetries has been tackled in the image processing and pattern analysis literature since the original works of Atallah [3] and Friedberg [17]. Nevertheless, it should be emphasized that there has long been interest in characterizing the symmetries of objects in biology, physics, and mathematics [40, 9]. Algorithms proposed in the image analysis literature on automatic detection of image symmetries can be classified with respect to their several characteristics. First of all, most of the algorithms can only cope with one type of image symmetry and typically this is reflectional symmetry [3], [17], [34], [43, 10, 25]. An attempt to detect both types of symmetry has been made in [24, 33]. A second important characteristic of symmetry detection algorithms are the constrains that are made on the image model. Hence, whether an image is a simple binary polyhedral object or just a collection of landmark points, or a general grey-level image function. Furthermore,

some algorithms use a continuous image model and additionally it has been assumed that the observed image is noise-free. Additionally, certain algorithms assume in advance that the image is symmetric, whereas others are able to detect the symmetry property. Unfortunately, most existing algorithms in the image analysis literature use a continuous and noise-free image model and often make a priori assumption that the underlying image is symmetric, whereas others are able to detect the symmetry type without such advance information.
In particular, in [24] an algorithm for detecting both types of symmetries is proposed that makes use of the continuous polar representation $\tilde{f}(\rho, \theta)$ of the input, noise-free image function $f(x, y)$. This representation is then used to define the so-called angular correlation, which measures the correlation between images in the angular direction. It is shown that if $\tilde{f}(\rho, \theta)$ is rotationally symmetric of order d then the angular correlation is a periodic function whose fundamental period is $2\pi/d$. Regarding images with reflectional symmetry it has been proved that the tilt of the symmetry axis can be obtained from the angular correlation between $\tilde{f}(\rho, \theta)$ and its flipped version $\tilde{f}(\rho, -\theta)$. The implementation of the proposed method for digital images is carried out by computing the pseudopolar Fourier transform. The accuracy of the algorithm is assessed via simulation examples. The Fourier domain approach to symmetry detection is also presented in [32, 10]. These detection methods are based on the symmetry preservation property of Fourier transform of symmetric images. A continuous and noise-free image model is assumed. In the aforementioned contributions the a priori existence of a fixed type symmetry is required and detection procedures are based on a direct evaluation of the given symmetry parameters, i.e., the tilt of the symmetry axis (for reflectional symmetry) and the fraction of cycles which induces symmetry (for rotational symmetry). Hence, no rejection of symmetry with a given level of confidence is possible. An algorithm for detecting local reflectional symmetry based on a local symmetry operator is demonstrated in [25]. Taking into account all such local operators a global reflectional symmetry is found by an optimisation method utilizing genetic algorithms. A continuous image model defined on a circular domain is used. No discretization and noise effects are examined. Let us also mention the contribution [44], where the importance of symmetry detection is strongly stressed, and algorithms for the detection of points of local symmetry in an image using phase information are proposed. In the seminal paper [3], the combinatorial approach for finding all symmetry relations in an image consisting of n objects such as circle, lines, points is proposed. In [15] the symmetry problem is discussed for objects represented by a set of labelled landmarks. [34] considers reflectional symmetry and aims at finding all axis of reflection symmetry of a planar image, using maximisation of a specifically defined coefficient of symmetry. The algorithm is robust to mild noise, but it is a priori assumed that the image has the required symmetry. The author further stresses that it would be desirable in the presence of noise to have methods to investigate whether an image has certain symmetries in the first place. In [43] a method for estimating the plane of reflection symmetry of three dimensional objects is examined. As for rotational symmetry, [27] proposes a method for estimating the rotation angle, which is based on Zernike moments. However, the authors do not study any convergence aspects of the algorithms and confine their discussion to noise-free images. Further, [17] gives a method for detecting the skewed axis of symmetry of bilaterally symmetric objects. Finally, [39] studies a related problem whether two images only differ by some (symmetry) transformation.
Though symmetry can be examined from different point of views, in this paper statistical aspects of spatial symmetry are studied. Hence, we investigate a rarely (to our best knowledge) studied problem of finding whether a digital version of the continuous image which is observed in the presence of noise actually has a certain type of (global) symmetries. Apparently, even

if symmetries are present, due to random noise these can only be observed approximately, and the question arises whether the departure from symmetry is due to noise or actually due to an asymmetric image. Hence, our goal is to construct rigorous statistical tests for testing rotational and reflection symmetries in a planar grey-level image. Before we discuss our detection method more specifically, we also review parts of the relevant statistics literature on symmetry testing.

Questions of symmetry are relevant in many statistical models. Such symmetry can simplify statistical inference, or it might be of interest in itself. For example, in linear as well as in nonparametric regression models, it is important to know whether the error distribution is symmetrical around zero, since this can increase the efficiency of estimation (cf. [6]) as well as the quality of asymptotic approximations by the normal distribution (cf. [18], p. 229). Therefore, in [16] and [14] tests for symmetry of the error distribution in linear and nonparametric regression, respectively, are proposed. Furthermore, nonparametric tests for symmetry of an unknown regression function (cf. [30]), or of an unknown density (cf. [1]) have also been proposed. In [2], tests for symmetry about unknown parameters are constructed.

However, there seem to be no methods available in the statistics literature for testing symmetries of a nonparametric regression function relevant to the image analysis setting, i.e., when one observes a noisy version of an image function recorded on a regular square grid. In this paper the image plane is defined to be the unit disk, and we use a class of radial orthogonal functions, often referred to as Zernike functions, to design our testing procedures. Hence, we propose a systematic approach for testing image symmetries utilizing the Zernike coefficients (Zernike moments), i.e., the Fourier coefficients of the expansion of the image function into the Zernike functions. The proposed test statistics are constructed by expressing the symmetry condition in terms of restrictions on the Zernike moments [42]. The statistics take form of empirical counterpart of the L_2 distance between the original image and its transformed version obtained by a certain symmetry transformation. The established limit theorems allow us to design rigorous methods for testing symmetries of planar images observed in the presence of noise over a grid of pixels. We derive the asymptotic distributions of the test statistics both under the hypothesis of symmetry as well as under fixed alternatives. The former result is used to construct asymptotic level α tests for lack of symmetry, whereas the latter result can be used to estimate the power of these tests, or to construct tests for validating the symmetry of the image. The tests are nonparametric as they do not need any prior knowledge of the image shape and content. They are based on the region-based orthogonal Zernike moment descriptors and therefore in the case of rejecting the null hypothesis on the image symmetry they can still be used as a reconstruction method. This allows us to obtain a great deal of information about the image even if it has been classified to be non-symmetrical. This is a unique property of our testing method not shared by the existing algorithms for detecting symmetry in grey-level images. Our theory models the performance of the detection procedures on grids which become increasingly fine. Furthermore, we extend our methodology to the case of testing joint symmetries, i.e., symmetry with respect to several transformations. We verify the quality of the asymptotic approximations in extensive simulation studies. It is shown that the tests perform well, both in terms of keeping the nominal level under the hypothesis of symmetry, as well as in terms of power under departures from symmetry. Furthermore, we apply our methods to the problem of testing symmetry of the PSF in confocal microscopy.

Details of the all technical proofs of the presented theorems can be found in the accompanying technical report [4].

2 The Zernike Orthogonal Basis and Image Reconstruction

The Zernike polynomials were introduced as an orthogonal and rotationally invariant basis of polynomials on the disc in order to model aberrations in optical systems [46]. Since then, Zernike functions and their corresponding moments have been found important in numerous applications ranging from pattern recognition, shape analysis, optical engineering, medical imaging to describing aberrations in the human eye [41], [5], [28, 23]. In [31, 32] studies how accurately an image can be reconstructed from a finite number of Zernike moments, given that discrete observations without noise are available were conducted. [45] describes a high precision algorithm for computing Zernike moments. A survey of methods of moments in image reconstruction is given in [35]. In [26], the statistical properties of an estimation procedure in positron emission tomography based on the Zernike moments is investigated.

A. Zernike Polynomials

The Zernike orthogonal polynomials are given by

$$V_{pq}(x,y) = R_{pq}(\rho)\, e^{iq\theta}, \quad (x,y) \in D, \tag{1}$$

where $\rho = \sqrt{x^2+y^2}$, $\theta = \arctan(y/x)$, i is the imaginary unit, and $R_{pq}(\rho)$ is the radial Zernike polynomial given explicitly by

$$R_{pq}(\rho) = \sum_{l=0}^{(p-|q|)/2} \frac{(-1)^l (p-l)!\rho^{p-2l}}{l!\big((p+|q|)/2-l\big)!\big((p-|q|)/2-l\big)!}.$$

The indices (p,q) have to satisfy

$$p \geq 0, \quad |q| \leq p, \quad p-|q| \quad \text{even}, \tag{2}$$

we will call such pairs (p,q) admissible. The Zernike polynomials satisfy the following orthogonality relation

$$\iint_D V_{pq}(x,y) V^*_{p'q'}(x,y)\, dx\, dy = \pi/(p+1)\delta_{pp'}\delta_{qq'},$$

where * denotes complex conjugation and $\delta_{pp'}$ is the Kronecker delta. This implies that

$$\|V_{pq}\|^2 = \pi/(p+1) = n_p, \tag{3}$$

where $\|\cdot\|$ is the norm on $L_2(D)$. In [8], the Zernike polynomials are characterized as the unique orthogonal basis of $L_2(D)$ consisting of invariant polynomials of the general form (1), which contain a polynomial for every admissible pair (p,q) in (2), where p is the degree of $R_{pq}(\rho)$ and q is the index of angular dependence.

B. Function Approximation

Since the family $\{V_{pq}(x,y)\}$ for admissible (p,q) forms a complete and orthogonal system in $L_2(D)$, we can expand a function $f \in L_2(D)$ into the following orthogonal series

$$f(x,y) = \sum_{p=0}^{\infty} \sum_{q=-p}^{p} n_p^{-1}\, A_{pq}(f) V_{pq}(x,y), \tag{4}$$

where here and in all the following the summation is only taken over admissible pairs (p, q). The norming factor n_p^{-1} arises due to (3), and the Zernike coefficient $A_{pq}(f)$ is defined by

$$A_{pq}(f) = \iint_D f(x, y)\, V_{pq}^*(x, y)\, dx\, dy.$$

Introducing the notation $\tilde{f}(\rho, \theta) = f(\rho\cos\theta, \rho\sin\theta)$ for a function $f \in L_2(D)$, and by using polar coordinates one obtains

$$A_{pq}(f) = 2\pi \int_0^1 c_q(\rho, f)\, R_{pq}(\rho)\, \rho\, d\rho, \tag{5}$$

where

$$c_q(\rho, f) = \frac{1}{2\pi} \int_0^{2\pi} \tilde{f}(\rho, \theta) e^{-iq\theta}\, d\theta.$$

C. Image Reconstruction

The image observational model we will use in this paper is as follows. Let $f \in L_2(D)$ and suppose that we have data

$$Z_{i,j} = f(x_i, y_j) + \epsilon_{i,j}, \quad (x_i, y_j) \in D, \quad 1 \le i, j \le n, \tag{6}$$

where the noise process $\{\epsilon_{i,j}\}$ is an i.i.d. random sequence with zero mean, finite variance $E\epsilon_{i,j}^2 = \sigma^2$ and finite fourth moment. We assume that the data are observed on a symmetric square grid of edge width Δ, i. e. $x_i - x_{i-1} = y_i - y_{i-1} = \Delta$ and $x_i = -x_{n-i+1}$, $y_i = -y_{n-i+1}$. Note that n is of order $1/\Delta$. The design is illustrated in Figure 1. Note that along the boundary of the disc, some lattice squares are included and some are excluded. When reconstructing $f(x, y)$, this gives rise to an additional error, referred to as geometric error [38] . Throughout this paper the geometric error will be represented by the factor γ, which can be evaluated, see [38], to be equal $\gamma = 285/208$. In the following we shall work with a discretized version of the Zernike polynomials, since we observe the image function $f(x, y)$ in model (6) only on the discrete grid of points $\{(x_i, y_j),\, i, j = 1, \ldots, n\}$. Consider the weights

$$w_{pq}(x_i, y_j) = \iint_{\Pi_{ij}} V_{pq}^*(x, y)\, dxdy, \tag{7}$$

where $\Pi_{ij} = [x_i - \frac{\Delta}{2}, x_i + \frac{\Delta}{2}] \times [y_j - \frac{\Delta}{2}, y_j + \frac{\Delta}{2}]$ denotes the pixel centered at (x_i, y_j). Another, even simpler version of the weights is

$$w_{pq}(x_i, y_j) = \Delta^2 V_{pq}^*(x_i, y_j). \tag{8}$$

The expansion (4) can be used to construct a truncated series estimator for $f(x, y)$ in model (6). To this end estimate the Zernike coefficient $A_{pq}(f)$ by

$$\hat{A}_{pq} = \sum_{(x_i, y_j) \in D} w_{pq}(x_i, y_j) Z_{i,j}, \tag{9}$$

where the weights are given by (7) or by (8). An estimate of the image function $f(x, y)$ is then given by

$$\hat{f}_N(x, y) = \sum_{p=0}^{N} \sum_{q=-p}^{p} n_p^{-1} \hat{A}_{pq}(f) V_{pq}(x, y), \tag{10}$$

where N is a smoothing parameter which determines the number of terms in the truncated series. The mean integrated square error properties of $\hat{f}_N(x, y)$ are discussed in [38], for general information on truncated series estimators see, e.g., [20].

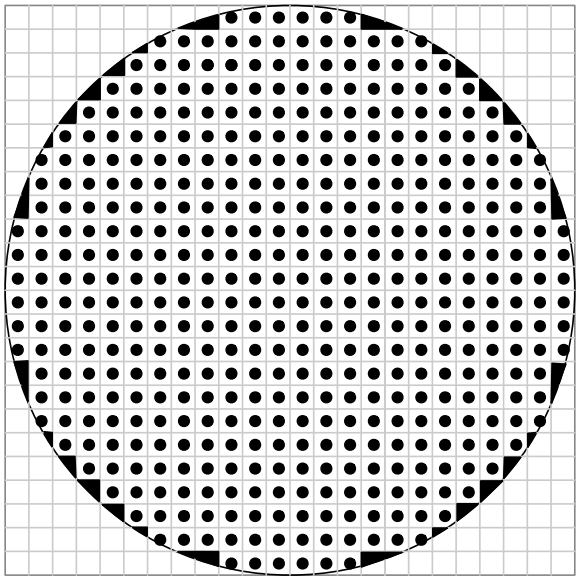

Figure 1: Design of the observational model.

3 Testing Rotational Symmetries

In this section we discuss how to test for rotational symmetries of $f \in L_2(D)$. We consider both d-fold rotations as well as rotational invariance, the limit case $d = \infty$.

A. d-Fold Rotations

Let us consider a rotation r_d by an angle of $2\pi/d$ for $d \in \mathbb{N}$. Since

$$\widetilde{(r_d f)}(\rho, \theta) = \tilde{f}(\rho, 2\pi/d + \theta), \tag{11}$$

from (5) it easily follows that

$$A_{pq}(r_d f) = e^{2\pi i q/d} A_{pq}(f). \tag{12}$$

Now consider the hypothesis

$$H^{r_d} : r_d f = f, \tag{13}$$

that the function f is invariant under the rotation r_d. Expanding both sides of (13) into a series with respect to the Zernike basis, we see that (13) is equivalent to $A_{pq}(r_d f) = A_{pq}(f)$ for all admissible pairs (p, q). In view of (12), this is equivalent to

$$H^{r_d} : A_{pq}(f) = e^{2\pi i q/d} A_{pq}(f) \quad \text{for all admissible pairs } (p, q).$$

Therefore, a natural way to test the hypothesis H^{r_d} is via the statistic

$$T_N^{r_d} = \frac{1}{4} \sum_{p=0}^{N} \sum_{q=-p}^{p} n_p^{-1} \left|1 - e^{2\pi i q/d}\right|^2 \left|\hat{A}_{pq}\right|^2, \tag{14}$$

where the norming factor $1/4$ is used for convenience. It is worth noting that $T_N^{r_d}$ represents the empirical version of the truncated L_2 distance between $f(x,y)$ and its orthogonal projection $r_d f(x,y)$ onto all images being symmetric with respect to $d-$fold rotations. Indeed, by Parseval's formula we have

$$\|f - r_d f\|^2 = \sum_{p=0}^{\infty} \sum_{q=-p}^{p} n_p^{-1} \left|1 - e^{2\pi i q/d}\right|^2 \left|A_{pq}\right|^2.$$

We will study explicitly two important special cases, $d = 2$, i.e., rotation by π, and $d = 4$, rotation by $\pi/2$. In principle, one could derive similar results for general rotations by the angle $2\pi/d$. However, in this case, additional technical difficulties may arise since the discrete grid points $\{(x_i, y_j)\}$ need no longer be invariant under r_d. To obtain an approximate invariance one should apply some interpolation methods, see [45].

Since for $d = 2$ we have $e^{i\pi q} = (-1)^{|q|}$, the terms in (14) for even q (or equivalently even p) vanish. Therefore, the statistic in this case reads

$$T_N^{r_2} = \sum_{p=0,p\ odd}^{N} \sum_{q=-p}^{p} n_p^{-1} \left|\hat{A}_{pq}\right|^2. \tag{15}$$

The following theorem presents the asymptotic distribution of the statistic $T_N^{r_2}$ under the hypothesis H^{r_2} as well as under fixed alternatives.

Theorem 1. *Under the hypothesis $H^{r_2} : r_2 f = f$, if $\Delta \to 0$, $N \to \infty$ such that $\Delta N^7 \to 0$, we have that*

$$\frac{1}{\Delta^2 \sqrt{a(N)}} \left(T_N^{r_2} - \sigma^2 \Delta^2 a(N)\right) \xrightarrow{\mathcal{L}} N(0, 2\sigma^4), \tag{16}$$

where $\xrightarrow{\mathcal{L}}$ denotes convergence in distribution, $N(0,\sigma^2)$ is the normal law with mean zero and variance σ^2 and

$$a(N) = \begin{cases} N(N+2)/4 & : \quad N \text{ even}, \\ (N+1)(N+3)/4 & : \quad N \text{ odd}. \end{cases} \tag{17}$$

Under a fixed alternative $f \neq r_2 f$, suppose that $f \in C^s(D)$ for $s \geq 2$. If $\Delta N^{2s+1} \to \infty$ and $N^{3/2}\Delta^{\gamma-1} \to 0$, where $\gamma = 285/208$ is the factor controlling the geometric error, we have that

$$\frac{1}{\Delta} \left(T_N^{r_2} - \|f - r_2 f\|^2/4\right) \xrightarrow{\mathcal{L}} N(0, \sigma^2 \|f - r_2 f\|^2). \tag{18}$$

The proof of Theorem 1 can be found in the Appendix.

Remark 1. Note that different rates appear under the hypothesis in (16) and under fixed alternatives in (18). This phenomenon is by now rather well known for nonparametric tests (cf. e.g. [14]). Here it occurs since $T_N^{r_2}$ is, under the hypothesis, a quadratic statistic, but under a fixed alternative an additional linear term arises which dominates the asymptotics. There is extensive work on rate optimal testing in the statistic literature, both against linear local alternatives as well as uniformly against certain function classes of local alternatives (cf. [21] for a comprehensive discussion in the context of testing for the parametric form of a regression function). We constructed the test statistic in (14) not with such theoretical optimality questions in mind, but with the aim of providing a simple and transparent test, which also directly leads to estimators of the image, both in case of symmetry and under the alternative of no symmetry.

Remark 2. Let us now discuss implementation issues related with Theorem 1, which can be used to construct an asymptotic level α test for the hypothesis H^{r_2}. The hypothesis H^{r_2} is rejected if

$$T_N^{r_2} > u_{1-\alpha}\Delta^2\sqrt{2a(N)}\hat{\sigma}^2 + \Delta^2 a(N)\hat{\sigma}^2. \tag{19}$$

Here $u_{1-\alpha}$ denotes the $1-\alpha$ quantile of the standard normal distribution, and $\hat{\sigma}^2$ is a nonparametric estimator of the variance σ^2. For example, one can use a difference based estimator like

$$\hat{\sigma}^2 = \frac{1}{C(\Delta)} \sum_{(x_i,y_j)\in D} \frac{1}{4}\Big(\big(Y_{i,j} - Y_{i+1,j}\big)^2 + \big(Y_{i,j} - Y_{i,j+1}\big)^2 \Big), \tag{20}$$

where the sum is taken over all $(x_i, y_j) \in D$ where $(x_{i+1}, y_j) \in D$ and $(x_i, y_{j+1}) \in D$, and $C(\Delta)$ is the number of terms in this restricted sum. One can show that if f is Lipschitz continuous, then $\hat{\sigma}^2 - \sigma^2 = O_P\big(\Delta\big)$. In this case, (16) continues to hold if σ^2 is replaced by the estimator $\hat{\sigma}^2$, and (19) is indeed an asymptotically valid level α test decision. For detailed information on difference-based variance estimators in higher dimensions see [36].

The asymptotic distribution (18) of the test statistic $T_n^{r_2}$ in (15) under a fixed alternative can be used in various ways. One is to estimate the power of the test. In fact, we have that for $\beta \in (0,1)$,

$$P\big(\hat{\sigma}\|f - r_2 f\|\Delta u_{1-\beta} + \|f - r_2 f\|^2/4 \le T_N^{r_2}\big) \approx \beta.$$

Using the decision rule (19), we see that for the power β we get asymptotically

$$\beta = 1 - \Phi\Big(\frac{\hat{\sigma}\Delta(u_{1-\alpha}\sqrt{2a(N)} + a(N))}{\|f - r_2 f\|} - \frac{\|f - r_2 f\|}{4\hat{\sigma}\Delta} \Big),$$

where Φ is the distribution function of the standard normal distribution. Observing that the first term in brackets tends to zero and then estimating $\|f - r_2 f\|$ by $2\sqrt{T_N^{r_2}}$, we get as an estimate for the power β

$$\hat{\beta} = 1 - \Phi\Big(- \frac{\sqrt{T_N^{r_2}}}{2\hat{\sigma}\Delta} \Big).$$

Another use of (18) is to validate the symmetry of f under r_2 by testing the hypothesis

$$H_t : \|f - r_2 f\| > t \quad \text{against} \quad K_t : \|f - r_2 f\| \le t,$$

for some $t > 0$. For further details on such testing problems we refer to [12].

Now let us consider testing for invariance under the rotation r_4 by an angle $2\pi/d$ with $d = 4$. Here, the factor $\big|1 - e^{2\pi i q/d}\big|^2$ in (14) becomes

$$\big|1 - i^q\big|^2 = \begin{cases} 4 & : \quad q \equiv 2 \bmod 4, \\ 0 & : \quad q \equiv 0 \bmod 4, \\ 2 & : \quad q \equiv 1, 3 \bmod 4. \end{cases}$$

Therefore, the statistic $T_N^{r_4}$ can be written as

$$T_N^{r_4} = \frac{1}{2} \sum_{p=0, p \ odd}^{N} \sum_{q=-p}^{p} n_p^{-1} \big|\hat{A}_{pq}\big|^2 + \sum_{p=0}^{N} \sum_{q \equiv 2 \bmod 4} n_p^{-1} \big|\hat{A}_{pq}\big|^2.$$

The asymptotic distribution of the statistic $T_N^{r_4}$ is established in the following theorem.

Theorem 2. *Under the hypothesis $H^{r_4} : r_4 f = f$, if $\Delta \to 0$, $N \to \infty$ such that $\Delta N^7 \to 0$, we have that*

$$\frac{1}{\Delta^2 \sqrt{a(N)/4 + b(N)}} \Big(T_N^{r_4} - \sigma^2 \Delta^2 \big(a(N)/2 + b(N) \big) \Big) \xrightarrow{\mathcal{L}} N\big(0, 2\sigma^4\big),$$

where $a(N)$ is given in (17), and $b(N)$ is equal to the number of admissible (p, q) with $q \equiv 2$ mod 4 and $p \leq N$.
Under a fixed alternative $f \neq r_4 f$, suppose that $f \in C^s(D)$ for $s \geq 2$. If $\Delta N^{2s+1} \to \infty$ and $N^{3/2}\Delta^{\gamma - 1} \to 0$, where $\gamma = 285/208$ is the geometric error factor, we have that

$$\frac{1}{\Delta} \big(T_N^{r_4} - \|f - r_4 f\|^2/4 \big) \xrightarrow{\mathcal{L}} N(0, \sigma^2 \|f - r_4 f\|^2).$$

The proof of Theorem 2 is similar to that of Theorem 1 and is therefore omitted, see [4] for details. It is worth noting that in $T_N^{r_4}$, more Zernike coefficients are needed than in $T_N^{r_2}$, which is to be expected since H^{r_4} imposes more restrictions than H^{r_2}, which have to be checked.

B. Testing Radiality

Next we wish to design a test for rotational invariance of $f(x, y)$, which means that $\tilde{f}(\rho, \theta) = g(\rho)$ is a function of the radius ρ only. Expressed in terms of the Zernike polynomials, a function $f \in L^2(D)$ is rotationally invariant if and only if

$$A_{pq}(f) = 0 \text{ for every } q \neq 0. \tag{21}$$

This is easily deduced from the definition of the Zernike coefficients (5), see also [38]. The orthogonal projection $Rot_\theta(f)$ of a function $f \in L^2(D)$ onto the space of rotationally invariant functions is therefore given by

$$Rot_\theta(f)(x, y) = \sum_{p=0,\, p \text{ even}}^{\infty} n_p^{-1} A_{p,0}(f) V_{p,0}(x, y),$$

and the L_2 distance between f and $Rot_\theta(f)$ is

$$\|f - Rot_\theta(f)\|^2 = \sum_{p=0}^{\infty} \sum_{q=-p, q\neq 0}^{p} n_p^{-1} |A_{pq}(f)|^2. \tag{22}$$

Consider the hypothesis H^{rot} that the image f is rotationally invariant,

$$H^{rot} : f = Rot_\theta(f).$$

Then, in order to test H^{rot}, it is natural to consider the statistic being the estimated and truncated version of (22)

$$T_N^{rot} = \sum_{p=1}^{N} \sum_{q=-p, q\neq 0}^{p} n_p^{-1} \big| \hat{A}_{pq} \big|^2.$$

The asymptotic distribution of T_N^{inv} is presented in the following theorem.

Theorem 3. *Under the hypothesis H^{rot}, if $\Delta \to 0$, $N \to \infty$ such that $\Delta N^7 \to 0$, we have that*

$$\frac{1}{\Delta^2\sqrt{a(N)}}\big(T_N^{rot} - \sigma^2\Delta^2 a(N)\big) \xrightarrow{\mathcal{L}} N(0, 2\sigma^4), \tag{23}$$

where

$$a(N) = \begin{cases} (N^2+2N)/2 & : \ N \text{ even}, \\ (N+1)^2/2 & : \ N \text{ odd}. \end{cases}$$

Under a fixed alternative $f \neq Rot_\theta(f)$, suppose that $f \in C^s(D)$ for $s \geq 2$. If $\Delta N^{2s+1} \to \infty$ and $N^{3/2}\Delta^{\gamma-1} \to 0$, where $\gamma = 285/208$ is the geometric error factor, we have that

$$\frac{1}{\Delta}\big(T_N^{rot} - \|f - Rot_\theta(f)\|^2\big) \xrightarrow{\mathcal{L}} N(0, 4\sigma^2\|f - Rot_\theta(f)\|^2). \tag{24}$$

For the proof of Theorem 3 see [4]. Testing procedures based on Theorems 2 and 3 can now be implemented in a completely analogous fashion as discussed in Remark 2.

C. General Rotations

In this section we discussed tests for invariance under specific rotations, namely d-fold rotations and rotational invariance. However, these are essentially all possibilities for rotational invariance in two dimensions. Let us consider general rational rotations by an angle of $2d_1\pi/d_2$ for $d_1, d_2 \geq 1$ coprime. Then the condition of invariance of a function under the rotation $2d_1\pi/d_2$ is equivalent to invariance under $2\pi/d_2$, since both reflections generate the same finite groups of rotations. As for an irrational rotation, say by $2x\pi$, x irrational, it is well known that the orbit of any point on a circle of radius ρ is dense on this circle. Hence, invariance under an irrational rotation is very close to rotational invariance (for continuous image functions it is equivalent).

4 Testing Reflection and Joint Symmetries

A. Reflections

In this section we examine the problem how to test that $f \in L_2(D)$ in model (6) is symmetric with respect to certain reflections. First let us consider the reflection τ at the y-axis, defined by $\tau f(x,y) = f(-x,y)$, $(x,y) \in D$. In polar coordinates, this is

$$\widetilde{(\tau f)}(\rho,\theta) = f\big(\rho\cos(\pi-\theta), \rho\sin(\pi-\theta)\big) = \tilde{f}(\rho, \pi-\theta).$$

Simple algebra shows that in (5), $c_q(\rho, \tau f) = (-1)^{|q|}c_{-q}(\rho, f)$. Since also $R_{pq}(\rho) = R_{p,-q}(\rho)$, we get $c_q(\rho,\tau f) = (-1)^{|q|}c_{-q}(\rho,f)$ and that $R_{pq}(\rho) = R_{p,-q}(\rho)$, therefore in view of (5) we have

$$A_{pq}(\tau f) = (-1)^{|q|}A_{p,-q}(f). \tag{25}$$

Now consider the hypothesis that the image $f(x,y)$ is invariant under τ, i.e.

$$H^\tau : \tau f = f,$$

which using (25) can be expressed in terms of Zernike coefficients as $A_{pq}(f) = (-1)^{|q|}A_{p,-q}(f)$ for admissible (p,q). Therefore a natural test statistic is

$$T_N^\tau = \sum_{p=0}^{N}\sum_{q=-p}^{p} n_p^{-1}\big|\hat{A}_{pq} + (-1)^{|q|+1}\hat{A}_{p,-q}\big|^2.$$

The following theorem gives the asymptotic distribution of T_N^τ under the hypothesis H^τ as well as under fixed alternatives.

Theorem 4. *Under the hypothesis $H^\tau : \tau f = f$, if $\Delta \to 0$, $N \to \infty$ such that $\Delta N^7 \to 0$, we have that*

$$\frac{1}{\Delta^2\sqrt{(N+1)(N+2)}}\big(T_N^\tau - \sigma^2\Delta^2(N+1)(N+2)\big) \xrightarrow{\mathcal{L}} N(0, 8\,\sigma^4). \tag{26}$$

Under a fixed alternative $\tau f \neq f$, suppose that $f \in C^s(D)$ for some $s \geq 2$. If $\Delta N^{2s+1} \to \infty$ and $N^{3/2}\Delta^{\gamma-1} \to 0$, where $\gamma = 285/208$ is the geometric error factor, we have that

$$\frac{1}{\Delta}\big(T_N^\tau - \|f - \tau f\|^2\big) \xrightarrow{\mathcal{L}} N(0, 16\sigma^2\|f - \tau f\|^2). \tag{27}$$

The proof of Theorem 4 can be found in [4]. Similar test statistics and asymptotic results can in principle be deduced for reflections with respect to arbitrary axis through the origin. In particular, for reflection with respect to the x-axis or one of the diagonals, similar results hold true, since the design is also invariant under these reflections. Generally, however, one should estimate the tilt angle of the reflection axis and include that in our detection procedure, see [24] for the angular correlation approach for estimating the reflection axis angle.

B. Joint Symmetries

Now let us consider testing for joint symmetries, i.e., for symmetry with respect to several transformations. As an example consider invariance under the reflections at the x- and y-axis, now denoted by τ_x and τ_y, respectively. Since $\tau_x\tau_y = r_2$ and $r_2\tau_y = \tau_x$, the group generated by $\{\tau_x, \tau_y\}$ is the same as that generated by $\{\tau_y, r_2\}$. Therefore, one can also test for invariance with respect to the reflection τ_y and the rotation r_2. In general, a group generated by two reflections can always be generated by a reflection and a rotation.

Since we already have test statistics for the hypotheses H^{r_2} and H^{τ_y}, we could test the joint hypothesis $H^{\tau_y,r_2} = H^{r_2} \wedge H^{\tau_y}$ via a multiple testing procedure (cf. [22] for background on multiple testing). As an example, the Bonferroni procedure tests both hypotheses H^{r_2} and H^{τ_y} to the level $\alpha/2$. If at least one is rejected at this level, the compound hypothesis H^{τ_y,r_2} can be rejected at a level of α.

However, it is also of interest to construct a test statistic which directly tests the hypothesis H^{τ_y,r_2}, since such tests often outperform multiple testing procedures in terms of power. To this end let $L_2(\tau_y, r_2) \subset L_2(D)$ be the subspace of functions in $L_2(D)$ invariant under τ_y and r_2. Then the orthogonal projection π_{τ_y,r_2} of $f \in L_2(D)$ onto $L_2(\tau_y, r_2)$ is given by

$$\pi_{\tau_y,r_2}(f)(x,y) = \sum_{p \text{ even}} \sum_{q=-p}^{p} n_p^{-1}\Big(\frac{A_{pq}(f) + (-1)^{|q|}A_{p,-q}(f)}{2}\Big)V_{pq}(x,y).$$

The test statistic is now defined by estimating the distance $\|f - \pi_{\tau_y,r_2}f\|^2$. Expressing this in terms of Zernike coefficients leads to the test statistic

$$T_N^{\tau_y,r_2} = \sum_{p=0,p\ odd}^{N} \sum_{q=-p}^{p} n_p^{-1}\big|\hat{A}_{pq}\big|^2 + \frac{1}{4}\sum_{p=0,p\ even}^{N} \sum_{q=-p}^{p} n_p^{-1}\left|\hat{A}_{pq} + (-1)^{|q|+1}\hat{A}_{p,-q}\right|^2.$$

For this test statistic we have the following result.

n	σ	S/N	N_r
25	0.2	5	7
25	0.06	16.7	8
25	0.02	50	10
50	0.2	5	8
50	0.06	16.7	12
100	0.2	5	12

Table 1: Smoothing parameter N_r used for the estimator $\hat{f}_N(x,y)$ in the subsequent simulations. S/N gives the signal-to-noise ratio which we define as the ratio between the peak values of the test functions $\tilde{f}_1, \tilde{f}_2$ and the standard deviation σ.

Theorem 5. *Under the hypothesis $H^{\tau_y,r_2} : \tau_y f = f$ and $r_2 f = f$, if $\Delta \to 0$, $N \to \infty$ such that $\Delta N^7 \to 0$, we have that*

$$\frac{1}{\Delta^2\sqrt{a(N)}}\big(T_N^{\tau_y,r_2} - \sigma^2\Delta^2 a(N)\big) \xrightarrow{\mathcal{L}} N(0, 2\sigma^4),$$

where

$$a(N) = \begin{cases} \frac{(N+2)^2}{8} + \frac{N(N+2)}{4}, & : \ N \text{ even}, \\ \frac{(N+1)^2}{8} + \frac{(N+1)(N+3)}{4} & : \ N \text{ odd}. \end{cases}$$

Under a fixed alternative $f \neq r_2 f$ or $\tau_y f \neq f$, suppose that $f \in C^s(D)$ for $s \geq 2$. If $\Delta N^{2s+1} \to \infty$ and $N^{3/2}\Delta^{\gamma-1} \to 0$, where $\gamma = 285/208$ is the geometric error factor, we have that

$$\frac{1}{\Delta}\big(T_N^{\tau_y,r_2} - \|f - \pi_{\tau_y,r_2} f\|^2\big) \xrightarrow{\mathcal{L}} N(0, 4\sigma^2\|f - \pi_{\tau_y,r_2} f\|^2).$$

For the proof of Theorem 5 see [4].

5 Simulations

In this section we discuss the results of a simulation study of the proposed symmetry tests. We performed simulations with two target functions, which are given in polar coordinates by

$$\begin{aligned} \tilde{f}_1(\rho,\theta) &= \rho^2 \sin(4\theta), \\ \tilde{f}_2(\rho,\theta) &= \rho^2 \sin(5\theta). \end{aligned}$$

Note that $\tilde{f}_1$ is 2-fold rotational symmetric, (i.e. invariant under r_2, cf. (11)), whereas $\tilde{f}_2$ is not. In the subsequent simulations we use these two functions to demonstrate the performance of the test for rotational symmetry under the hypothesis H^{r_2} and under the alternative hypothesis when H^{r_2} does not hold. The test statistic $T_N^{r_2}$ defined in (15) is used here.

Figures 2 and 3 show reconstructions of $\tilde{f}_1$ and $\tilde{f}_2$ and the corresponding residuals, respectively, from estimation based on data with $n = 25, 100$ and with Gaussian noise of standard deviations $\sigma = 0.02, 0.2$. We show both the reconstructions where all Zernike polynomial with $p \leq N$ are used, as well as reconstructions assuming that H^{r_2} holds, i.e. where only polynomials for q even are used. In fact, under H^{r_2} we have $A_{pq}(f) = 0$ for q odd. Table

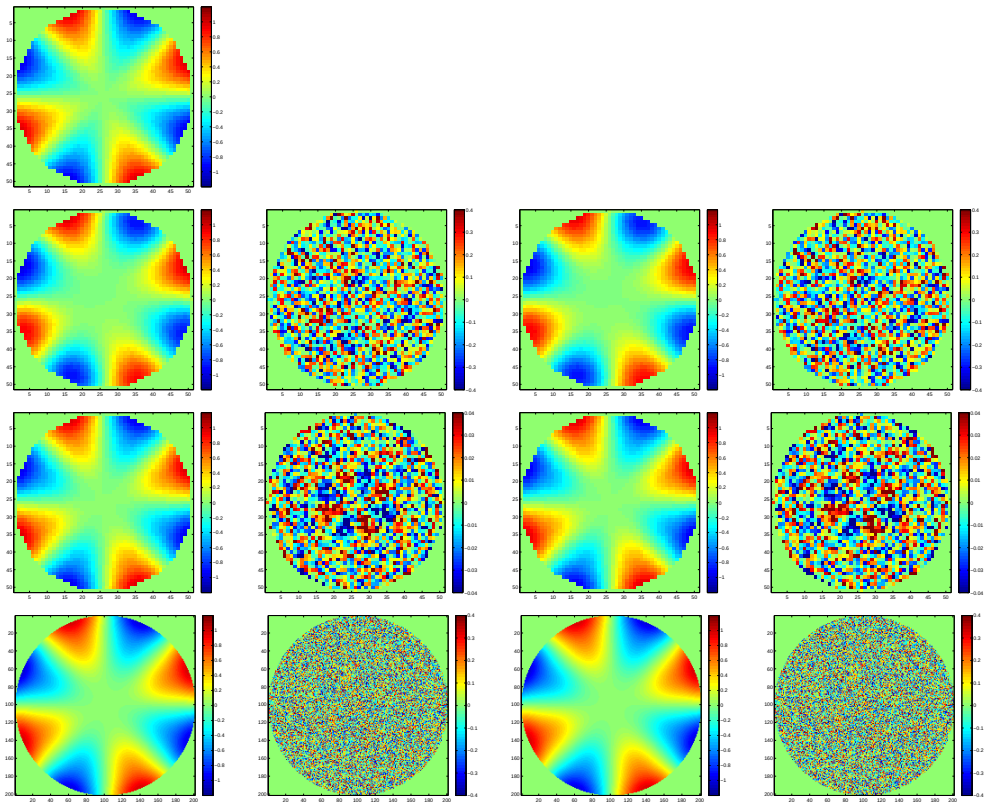

Figure 2: Reconstruction of $\tilde{f}_1$ (top row) from data with $n = 25, \sigma = 0.2$ (second row), $n = 25, \sigma = 0.02$ (third row) and $n = 100, \sigma = 0.2$ (bottom row). The plots in the second to bottom row, from left to right, show the estimate $\hat{f}_N$ based on all Zernike polynials, the residuals of this estimate, the estimate $\hat{f}_N^{r_2}$ based only on the polynomials with q even, and the residuals of the latter estimate.

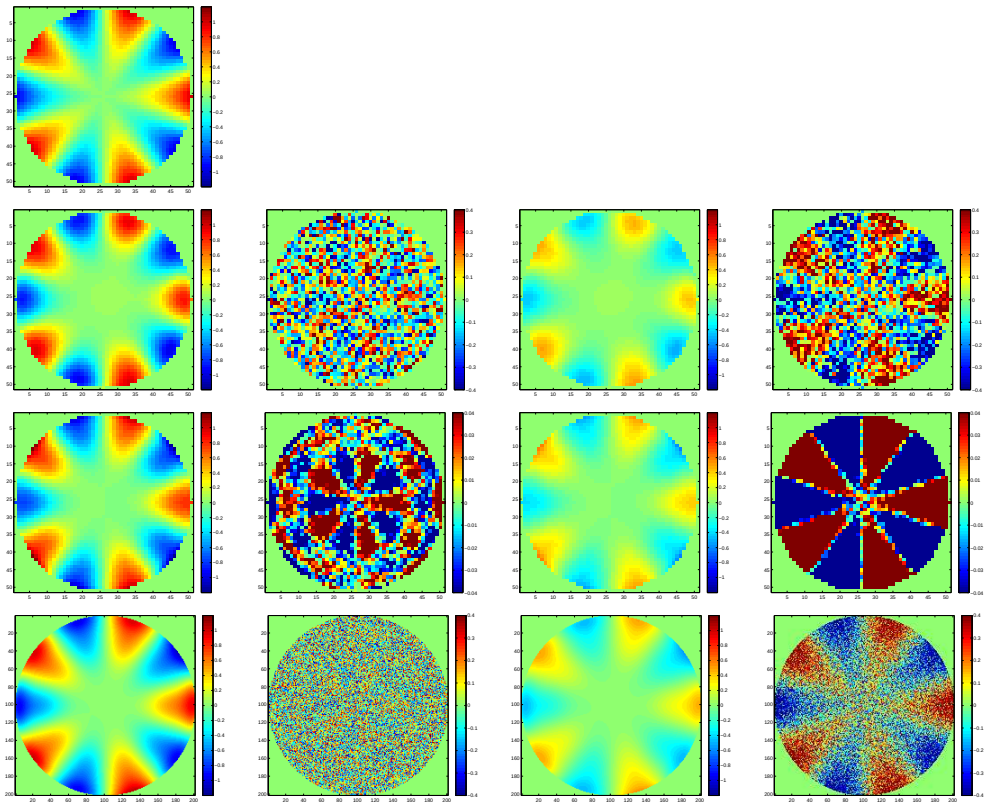

Figure 3: Reconstruction of $\tilde{f}_2$ (top row) from data with $n = 25, \sigma = 0.2$ (second row), $n = 25, \sigma = 0.02$ (third row) and $n = 100, \sigma = 0.2$ (bottom row). The plots in the second to bottom row, from left to right, show the estimate $\hat{f}_N$ based on all Zernike polynomials, the residuals of this estimate, the estimate $\hat{f}_N^{r_2}$ based only on the polymials with q even, and the residuals of the latter estimate.

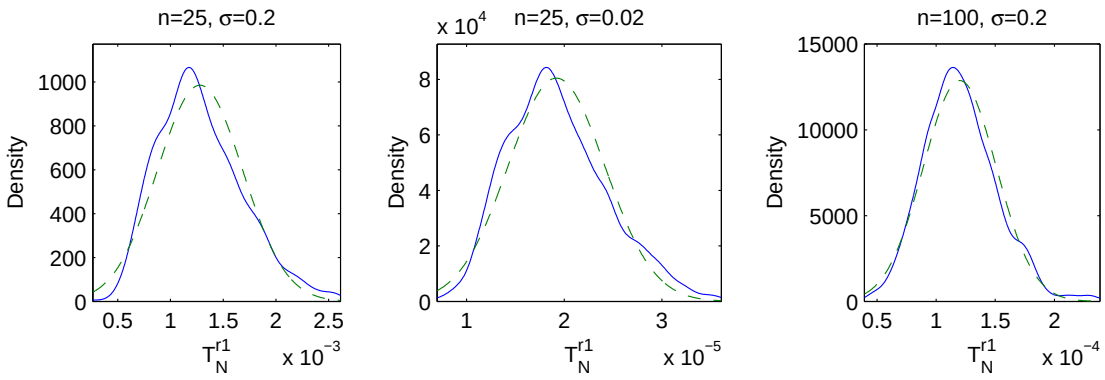

Figure 4: Simulated distribution (full curves) and asymptotic distribution (dashed curves) of the test statistic $T_N^{r_2}$ under the null hypothesis for (from left to right) $n = 25, \sigma = 0.2$, $n = 25, \sigma = 0.02$ and $n = 100, \sigma = 0.2$.

1 summarizes the smoothing parameters N used in these reconstructions (and in the subsequent simulations with the same set of parameters n, σ). The parameter N is chosen by the following data-driven method. In the first step, we have estimated the variance σ^2 with a difference estimator $\hat{\sigma}^2$ of type (20). Then we computed the estimator (10) for the data with $N = 1, 2, \ldots$ and evaluated the statistic

$$\mathcal{D}_N^2 := \frac{1}{n(D) - 1} \sum_{(x_i, y_j) \in D} \Big(\mathrm{Re}(Z_{i,j} - \hat{f}_N(x_i, y_j)) \Big)^2 ,$$

where $n(D) := \sum_{(x_i, y_j) \in D} 1$. Finally we chose the smoothing parameter N_r as the smallest N, such that $\mathcal{D}_N^2 \leq \hat{\sigma}^2$. We validated this strategy by comparing N_r to its L_2, L_1 and L_∞-optimal value for estimation of $\tilde{f}_1$ and $\tilde{f}_2$, which we can determine from the fact that in our simulations, the true function underlying the data is known. It turns out that the L_1 and L_∞-optimal smoothing parameters typically are within an interval of ± 2 from the L_2-optimal smoothing parameter, which is the same amount as the typical difference N_r from the L_2-optimal smoothing parameter. It is obvious from the figures that, whereas the reconstructions of $\tilde{f}_1$ appear feasible for all sets of parameters - both using all Zernike polynomials and using only the subset with q even - the reconstructions of $\tilde{f}_2$ suffer severely if only $2-$fold symmetric Zernike polynomials are used.
In the second part of our simulation study we simulated the distribution of the test statistic $T_N^{r_2}$ for testing for $2-$fold rotational symmetry, both with data generated under the null hypothesis and with data generated from $\tilde{f}_2$, for which H^{r_2} does not hold. Note that by linearity of the coefficient estimator (9) it is not relevant which function is chosen to generate data under H^{r_2}, as long as the function is strictly $2-$fold symmetric such as $\tilde{f}_1$.

Figures 4 and 5 show simulated distributions of the test statistic $T_N^{r_2}$ given in (15) for data generated from the functions $\tilde{f}_1$ (i.e. under H^{r_2}) and $\tilde{f}_2$ (i.e. under the corresponding alternative), respectively, from 1000 simulations each. Moreover, the dashed curves show the

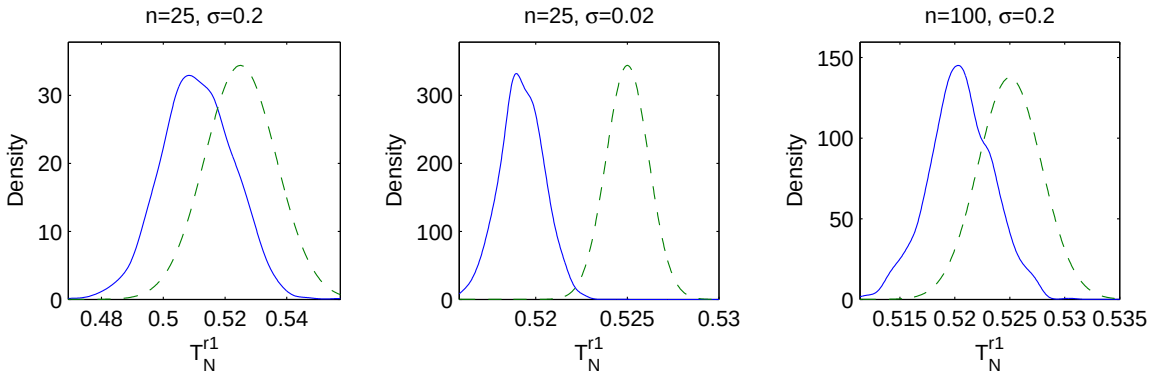

Figure 5: Simulated distribution (full curves) and asymptotic distribution (dashed curves) of the test statistic $T_N^{r_2}$ under the alternative hypothesis for (from left to right) $n = 25, \sigma = 0.2$, $n = 25, \sigma = 0.02$ and $n = 100, \sigma = 0.2$.

distributions computed from the asymptotic laws (16) and (18). The asymptotic mean and variance of the distribution of $T_N^{r_2}$ are attained well for all sets of parameters in the case of the simulations under H^{r_2}. Under the alternative (i.e. with data based on $\tilde{f}_2$) the asymptotic variance is also well-reproduced. For the expectation, which asymptotically is $\|f_2 - r_2 f_2\|^2$, there is an offset of order 5%, which is due to the fact that for the finite sample sizes considered here, there are still non-neglible remainder terms contributing to the distribution of $T_N^{r_2}$.

In the final part of the simulation study we have studied the performance of the test for data generated from $\tilde{f}_1$ (i.e. under H^{r_2}) and under a number of different alternatives based on $\tilde{f}_2$. In particular, we have considered linear combinations of $\tilde{f}_1$ and $\tilde{f}_2$ to determine the sensitivity of the test to violations of 2−fold rotational symmetry. To this end we have considered functions $\tilde{f}_{12,\kappa} = (1-\kappa)\tilde{f}_1 + \kappa\tilde{f}_2$ for $\kappa = 0.05$, 0.01 and 0.001. The critical values for the tests are determined from the simulated distribution of the test statistic based on $\tilde{f}_1$ shown in Figure 4. Table 2 gives the results from 1000 simulations each. The test appears to perform very well in the detection of asymmetry with respect to 2−fold rotational symmetry. First, the test keeps its nominal level well under the hypothesis H^{r_2} in the simulations with $\tilde{f}_1$. Second, a contribution of 1% of the function $\tilde{f}_2$, which is not 2−fold rotationally symmetric can be detected well if either at least the design size parameter $n \approx 100$, or if the signal-to-noise ratio is at least ≈ 17 (cf. table 1). Note from the simulations with $\tilde{f}_{12,0.001}$ that a contribution of 0.1% by the not 2−fold symmetric function $\tilde{f}_2$ can be detected only if $n = 100$, but not for smaller sample size, even for signal-to-noise ratio 50.

6 Testing for symmetry of the point-spread-function in confocal microscopy

In this section we apply the test for the 2−fold rotational symmetry to a problem related to assessing the quality of images from fluorescence nanoscale microscopy. Typically, for confocal fluorescence microscopic imaging, one observes count data representing observed image intensities on a two- (or three-dimensional), equidistant grid of design-points in the unit square. Here, we consider the two-dimensional case, where the design points are e.g.

True function	n	σ	20%	10%	5%
$\tilde{f}_1$	25	0.2	21.1%	10.3%	4.6%
$\tilde{f}_1$	25	0.02	17.8%	8.0%	3.7%
$\tilde{f}_1$	100	0.2	20.0%	10.7%	5.0%
$\tilde{f}_2$	25	0.2	100%	100%	100%
$\tilde{f}_2$	25	0.02	100%	100%	100%
$\tilde{f}_2$	100	0.2	100%	100%	100%
$\tilde{f}_{12,0.05}$	25	0.2	92.8%	86.6%	77.5%
$\tilde{f}_{12,0.05}$	25	0.06	100%	100%	100%
$\tilde{f}_{12,0.05}$	50	0.2	100%	100%	100%
$\tilde{f}_{12,0.01}$	25	0.2	21.7%	10.2%	4.6%
$\tilde{f}_{12,0.01}$	25	0.06	65.4%	51.7%	38.2%
$\tilde{f}_{12,0.01}$	25	0.02	100%	100%	100%
$\tilde{f}_{12,0.01}$	50	0.2	25.8%	21.5%	12.2%
$\tilde{f}_{12,0.01}$	50	0.06	98.0%	95.8%	88.3%
$\tilde{f}_{12,0.01}$	100	0.2	100%	100%	100%
$\tilde{f}_{12,0.001}$	25	0.02	19.5%	8.8%	4.4%
$\tilde{f}_{12,0.001}$	50	0.2	20.1%	10.5%	4.5%
$\tilde{f}_{12,0.001}$	50	0.06	23.0%	11.1%	3.6%
$\tilde{f}_{12,0.001}$	100	0.2	100%	100%	100%

Table 2: Effective fraction of rejection of the null hypothesis H^{r_2} in 1000 simulations of the test for 2−fold symmetry described in Theorem 1 for nominal levels 20%, 10% and 5%.

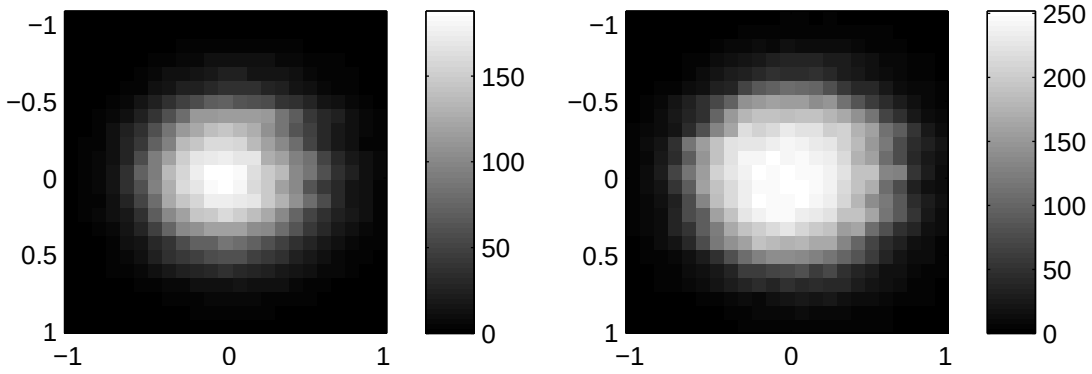

Figure 6: Images bead1 and bead2 acquired during to observation runs of HeLa cervix carcinoma cells with a Leica TCS laser scanning fluorescence microscope.

given by

$$z_{jk} = \left(\frac{j}{n}, \frac{k}{n}\right), \qquad -n \leq j, k \leq n.$$

Hence, the observations are $Y_{jk} = (K\theta)(z_{jk}) + \varepsilon_{jk}$, with

$$(K\theta)(z) = g * \theta(z) = \int_{\mathbb{R}^2} g(z-t)\theta(t)\, dt,$$

and where "$*$" represents the convolution of the "true" image $\theta \in L^2$ with the so-called point-spread-function (PSF) $g \in L^2$ of the microscope. Moreover, the standard model for the distribution of the photon count data Y_{jk} is that Y_{jk} is Poisson with the mean $(K\theta)(z_{jk})$, all independent.

The PSF represents the image of a point-source observed by the microscope and describes the blurring effect of the imaging process. It may be computed from the optical properties of the microscope, but the true (empirical) PSF can significantly deviate from its theoretic shape, e.g. due to imprecise alignment of elements in the optical path of the microscope, which frequently yields a non-symmetric PSF. Other frequent reasons for such asymmetries are inhomogeneities caused in the sample preparation, such as that the sample/mounting medium covership is not plane.

For confocal fluorescence microscopy, the convolution with the PSF amounts to a smoothing of the original image of the object, where typical smoothing scales are of order $\approx 100nm$, which often is of similar order as the size of (sub-)structures of interest in the target object. It is hence important to adjust (i.e. deconvolve) the observed image to recover the image of the target object. Hence, an exact knowledge of the PSF is evidently essential. One can in principle use the theoretically computed PSF. However, due to the miscellaneous reasons which can cause an asymmetric PSFs it is important to test whether this is empirically justified. For a rotationally symmetric optical system the corresponding PSF would be rotationally symmetric if the elements in the optical path and the detector plane were positioned perfectly well. On the other hand, reflection symmetry with respect to two orthogonal axes holds if, e.g., the detector plane was not in perfect agreement with the focal plane of the microscope (see [37, 29]). However, since these axes are in general not known, it is difficult to apply a test for reflection symmetry to an image of the PSF in practice, but we can instead test for $2-$fold rotational symmetry, which is an immediate consequence of the expected reflection symmetry. If the image is not $2-$fold rotation symmetric, it can also not be reflection symmetric w.r.t. two orthogonal axes.

We propose to test for an asymmetry in the empirical PSF by applying the test for $2-$fold rotation symmetry as follows. A standard method to observe the PSF in confocal microscopy is to include in an empty part of the imaged object slide or in a separate image a nano-sized bead, which is highly symmetric sphere of known size with a hard boundary, e.g. $50, 100$ or $200nm$ diameter, i.e. comparable in size to the full width at half maximum of the PSF. Hence, any asymmetry in the image of the bead indicates an imperfect alignment of the microscope optics.

Figure 6 shows two images of $200nm$ beads which have been acquired in two separate observational runs of fluorescently labeled living HeLa cells acquired with a confocal laser scanning microscope (Leica TCS). HeLa cells are a cervix cancer cell line and the object was labeled with the fluorescent dye Alexa 576 (red). The pixel size in both images is $21.3 \times 21.3nm$. We use subimages of the full microscopic images which actually show the beads. This yields

$n = 11$ for the design points. Here we have defined the design points such that the origin $(0, 0)$ of the coordinates coincides with the center-of-mass of the images of the beads. The signal-to-noise ratio of the images is $S/N \approx 20$ and $S/N \approx 14$ for bead1 and bead2, respectively. For a more detailed discussion of the HeLa cell data we refer to Bissantz et al. [7].
In the first step we choose the regularization parameter N_r as described in Section 5. Since the data are Poisson distributed and hence heteroscedastic, direct application of the difference estimator $\hat{\sigma}^2$ is difficult. We therefore cross-checked N_r by visual inspection, which confirmed the validity of the choice $N_r = 6$ and $N_r = 4$ for bead1 and bead2, respectively. In the second step we determine critical values for the test in the two scenarios (different both by $\hat{\sigma}^2$ and N_r) from simulated distributions of the test statistic with $T_N^{r_2}$ as in (15). Finally, applying the test for H^{r_2} to the images produced the following results. For bead1, the null hypothesis H^{r_2} was rejected even at the 5% level, whereas for bead2, it was not rejected, not even at the 20% level. This indicates that, whereas the data from the second observation run, where the image of bead2 was acquired, may well be deconvolved with the theoretical PSF, this is probably not a good strategy for the data from the first run. A possibility in this case is the estimation of the empirical PSF from the image of the bead; however this requires significant additional effort since the deconvolution is very sensitive e.g. to noise in the PSF. Finally, we mention that we have also tested both images for rotational invariance, which requires in particular a perfect alignement of the optical system, and of the detector with the focal plane, in addition to homogeneity of the prepared sample (e.g. of the mounting medium covership on the object slide). This (stronger) null hypothesis is rejected both for beat1 and bead2 even at the 5% level.

7 Concluding Remarks

In this paper we have considered the problem of testing for certain, prespecified symmetries in an image. However, one might also be interested in testing for reflection symmetry with respect to some unknown axis. In order to construct such a test, the first step consists in estimating the (possible) angle of the axis of reflection symmetry, and then as a second step inserting this estimator into the test statistic. Equivalently, we can realign the coordinate axis, so that the axis of symmetry is still the y-axis, and consequently the statistic T_N^τ can be used without any change.
If the angle of reflection symmetry under the hypothesis of actual symmetry is estimated at a parametric rate $O(\Delta)$, then we conjecture that the asymptotic distribution under the hypothesis H^τ remains unchanged. Indeed, the rate under the hypothesis in (26) is nonparametric, and if the angle is estimated at a faster rate, then this should not alter any asymptotic results. Such phenomena are known for related testing problems in the statistical literature when testing the parametric form of a regression function, see, e.g., [13]. Thus, the problem is to construct estimators for the reflection angle and prove that they have the required fast rate of convergence. Although, as described in the introduction, there are methods for estimation the angle of reflectional symmetry, they have not been studied so far from the theoretical point of view required for our nonparametric testing procedures. This interesting topic is beyond the scope of this paper and will be examined elsewhere.
Thus far, we have studied the problem of symmetry within a single image. The related two-sample problem is testing for equality of two images (such as left and right hands) up to symmetry transformation, where the images are observed with noise. For this problem, esti-

mation of the symmetry transformation would also be required as a first step, before plugging it into a test statistic.

Acknowledgements

Nicolai Bissantz acknowledges financial support of SFB 475 and the BMBF under project "INVERS" 03BIPAH4, and Hajo Holzmann acknowledges financial support from the Stifterverband der deutschen Wissenschaft and from the Juniorprofessorenprogramm Baden-Württemberg. The work of Mirosław Pawlak was supported by the NSERC. The authors would like to thank the associate editor and three anonymous referees for helpful comments, and Kathrin Bissantz for providing the record of biological data and her advice with its analysis.

8 Appendix

Before proving our theorems we need some auxiliary results. The first result gives a discretization error of the orthogonality property of the Zernike functions. The proof of this important result can be found in [4].

Lemma 1. *Let for some admissible pairs (p,q), (p',q'),*

$$I(\Delta) = \sum_{(x_i,y_j)\in D} w^*_{pq}(x_i,y_j) w_{p'q'}(x_i,y_j),$$

where $w_{pq}(x_i,y_j)$ is defined either in (7) or in (8). Then we have for some $c_1, c_2 > 0$ that

$$I(\Delta) = \Delta^2 n_p \delta_{pp'}\delta_{qq'} + c_1\Delta^{3+\alpha} + c_2\big(\sqrt{p+|q|}+\sqrt{p'+|q'|}\big)\Delta^{5/2}, \tag{28}$$

where α can be selected as $\alpha = 77/208 = 0,37019\ldots$.

The following lemma describes the discretization error of Parseval's formula when the true Zernike moment $A_{pq}(f)$ is estimated by $\hat{A}_{pq}(f)$.

Lemma 2. *Let $f \in C^s(D)$ – the class of functions having s continuous partial derivatives. Let $\hat{A}_{pq}(f)$ be the estimate of the Zernike coefficient defined in (9) and let*

$$S_N = \sum_{p=0}^{N}\sum_{|q|\le p} n_p^{-1}\big|E\hat{A}_{pq}(f)\big|^2.$$

Then we have

$$S_N = \|f\|^2 + O\big(N\Delta^{3/2} + N^{3/2}\Delta^{\gamma} + N^{-(2s+1)}\big)$$

with $\gamma = 285/208$.

Proof of Theorem 1. For admissible (p,q) with odd q, we have for the weights in both (7) and (8) that $w_{pq}(x_i,y_j) = (-1)^{|q|}w_{pq}(x_{n-i+1},y_{n-j+1})$. This is evident for (8). As for (7), first note that the rotate $-\Pi_{ij}$ of the pixel Π_{ij} is again a pixel, namely the pixel $\Pi_{n-i+1,n-j+1}$. Now use the fact that $w_{pq}(x_i,y_j) = A_{pq}\big(1_{\Pi_{ij}}\big)$ and (12), where $1_{\Pi_{ij}}$ is the indicator function of the set Π_{ij}. Then it follows that for admissible (p,q) with odd p,

$$\hat{A}_{pq}(f) = \sum_{(x_i,y_j)\in D} w_{pq}(x_i,y_j)\big(\bar{f}(x_i,y_j)+\epsilon_{i,j}\big),$$

where

$$\bar{f}(x,y) = \big(f(x,y) - f(-x,-y)\big)/2.$$

Set

$$m_{(ij),(kl)} = \sum_{(p,q)} n_p^{-1} w_{pq}(x_i,y_j)\, w^*_{pq}(x_k,y_l),$$

where here and for the rest of the proof all sums involving (p,q)'s are taken over admissible pairs with $0 \le p \le N$ and odd p. We obtain

$$\begin{aligned} T_N^{r_2} &= \sum_{(x_i,y_j),(x_k,y_l)\in D} \epsilon_{i,j}\,\epsilon_{k,l}\, m_{(ij),(kl)} + 2 \sum_{(x_i,y_j),(x_k,y_l)\in D} \bar{f}(x_i,y_j)\,\epsilon_{k,l}\, m_{(ij),(kl)} \\ &\quad + \sum_{(x_i,y_j),(x_k,y_l)\in D} \bar{f}(x_i,y_j)\,\bar{f}(x_k,y_l)\, m_{(ij),(kl)} \\ &= S_{1,N} + S_{2,N} + S_{3,N}. \end{aligned} \tag{29}$$

First assume that the hypothesis H^{r_2} is true. Then we have that $S_{2,N} = S_{3,N} = 0$, and we have to study $S_{1,N}$. Note that for the vectors $v_{pq} = \big(w_{pq}(x_i,y_j)\big)_{(x_i,y_j)\in D}$, from (28) it follows that

$$v_{pq}^{T,*} v_{p'q'} = \Delta^2 n_p \delta_{p,p'}\delta_{q,q'} + O\big(\Delta^{5/2}(p^{1/2} + |q|^{1/2} + p'^{1/2} + |q'|^{1/2})\big), \tag{30}$$

where the constant in $O()$ is independent of $p, q, p'q'$. The matrix of coefficients $M = \big(m_{(ij),(kl)}\big)_{(i,j),(k,l)\in D}$ can be written as

$$M = \sum_{(p,q)} n_p^{-1} v_{pq}\, v_{pq}^{T,*}. \tag{31}$$

Then using (30) we have for the expectation

$$\begin{aligned} ES_{1,N} = \sigma^2 trM &= \sigma^2 \sum_{(p,q)} n_p^{-1} tr(v_{pq}^{T,*} v_{pq}) \\ &= \sigma^2 \sum_{(p,q)} n_p^{-1}\big(\Delta^2 n_p + O\big(\Delta^{5/2}(p^{1/2} + |q|^{1/2})\big) \\ &= \sigma^2 \Delta^2 a(N) + O\big(\Delta^{5/2} N^{7/2}\big). \end{aligned} \tag{32}$$

where tr denotes the trace of a square matrix, and $a(N)$, the number of terms in the sum $\sum_{(p,q)}$ with odd p, is given by (17). Next decompose

$$\begin{aligned} S_{1,N} &= \sum_{(x_i,y_j)\in D} \epsilon_{i,j}^2\, m_{(i,j),(i,j)} + \sum_{(x_i,y_j)\neq(x_k,y_l)\in D} \epsilon_{i,j}\epsilon_{k,l} m_{(ij),(kl)} \\ &= S_{1,1,N} + S_{1,2,N}. \end{aligned}$$

First note that

$$ES_{1,2,N} = ES_{1,2,N}S_{1,1,N} = 0, \qquad ES_{1,N} = ES_{1,1,N},$$

as given in (32). Using the fact that $|w_{pq}(x,y)| \le \Delta^2$, we can estimate the variance of $S_{1,1,N}$ as follows:

$$\begin{aligned} Var\, S_{1,1,N} &\le E\big(\epsilon_{1,1}^2 - \sigma^2\big)^2 \sum_{(p_1,q_1)} \sum_{(p_2,q_2)} n_{p_1}^{-1}\, n_{p_2}^{-1} \\ &\quad \sum_{(x_i,y_j)\in D} |w_{p_1q_1}(x_i,y_j)|^2 |w_{p_2q_2}(x_i,y_j)|^2 = O\big(\Delta^6 N^6\big). \end{aligned} \tag{33}$$

Now let us evaluate the variance of $S_{1,2,N}$. Let D denote the diagonal matrix consisting of the diagonal elements of M. Then

$$\begin{aligned} Var\, S_{1,2,N} = 2\sigma^4 tr(M-D)^2 &= 2\sigma^4\big(trM^2 - trD^2\big) \\ &= 2\sigma^4 trM^2 + O(\Delta^6 N^6), \end{aligned} \tag{34}$$

where we used (33) in the last step. Furthermore

$$\begin{aligned} trM^2 &= \sum_{(p_1,q_1)} \sum_{(p_2,q_2)} n_{p_1}^{-1}\, n_{p_2}^{-1} |v_{p_1,q_1}^{T,*} v_{p_2,q_2}|^2 \\ &= \sum_{(p_1,q_1)} \sum_{(p_2,q_2)} n_{p_1}^{-1}\, n_{p_2}^{-1} \big(\Delta^2 n_p \delta_{p_1,p_2}\delta_{q_1,q_2} + O\big(\Delta^{5/2}(p_1^{1/2} + |q_1|^{1/2} + p_2^{1/2} + |q_2|^{1/2})\big)\big)^2 \\ &= \sum_{(p,q)} \Delta^4 + \sum_{(p,q)} n_p^{-1} \Delta^{9/2} O\big(p^{1/2} + |q|^{1/2}\big) \\ &\quad + \sum_{(p_1,q_1)} \sum_{(p_2,q_2)} n_{p_1}^{-1}\, n_{p_2}^{-1} \Delta^5 O\big(p_1 + |q_1| + p_2 + |q_2|\big) \\ &= a(N)\Delta^4 + O(\Delta^{9/2} N^{7/2}) + O(\Delta^5 N^7). \end{aligned}$$

Using this, (34) and $\Delta N^5 \to 0$, we get

$$Var\, S_{1,2,N} \sim 2\sigma^4 \Delta^4 a(N). \tag{35}$$

This is of higher order than the variance of $S_{1,1,N}$, therefore $S_{1,2,N}$ dominates the asymptotics. To evaluate its asymptotic distribution, we use Theorem 5.2 of de Jong [11]. To check condition 1) of this theorem, we compute

$$\begin{aligned} &\max_{(x_i,y_j)\in D} \sum_{(x_k,y_l)\in D} |m_{(ij),(kl)}|^2 \\ = &\max_{(x_i,y_j)\in D} \sum_{(p_1,q_1)} \sum_{(p_2,q_2)} n_{p_1}^{-1}\, n_{p_2}^{-1} w_{p_1q_1}(x_i,y_j) w_{p_2q_2}^*(x_i,y_j) \\ &\qquad \sum_{(x_k,y_l)\in D} w_{p_1q_1}^*(x_k,y_l) w_{p_2q_2}(x_k,y_l) \\ = &\; O(\Delta^6 N^6) = o\big(\Delta^4 N^2\big). \end{aligned}$$

Then condition 2) of Theorem 5.2 in [11] will be automatically satisfied (one could choose for $K(\Delta) = N$ in his condition 2), since the $\epsilon_{i,j}$ are i.i.d. In order to check his condition 3), we have to bound the spectral value of the matrix M defined in (31). First note that

$$M^2 = \sum_{(p_1,q_1)} \sum_{(p_2,q_2)} n_{p_1}^{-1} n_{p_2}^{-1} v_{p_1q_1} (v_{p_1q_1}^{*,T} v_{p_2q_2}) v_{p_2q_2}^{*,T}.$$

Applying (30) yields

$$M^2 = \Delta^2 M + \Delta^{5/2} \sum_{(p_1,q_1)} \sum_{(p_2,q_2)} n_{p_1}^{-1} n_{p_2}^{-1} v_{p_1q_1} v_{p_2q_2}^{*,T} O\big(\sqrt{p_1} + \sqrt{q_1} + \sqrt{p_2} + \sqrt{q_2}\big), \tag{36}$$

where the summation is taken over $(p_1,q_1) \neq (p_2,q_2)$. Let λ be an eigenvalue of the symmetric matrix M corresponding to the unit length eigenvector u. Noting that $M^2 u = \lambda^2 u$, we have from (36) that

$$\lambda^2 u = \Delta^2 \lambda u + \Delta^{5/2} \sum_{(p_1,q_1)} \sum_{(p_2,q_2)} n_{p_1}^{-1} n_{p_2}^{-1} v_{p_1q_1} v_{p_2q_2}^{*,T} u O\big(\sqrt{p_1} + \sqrt{q_1} + \sqrt{p_2} + \sqrt{q_2}\big).$$

Subtracting and taking the norm gives

$$\lambda^2 - \Delta^2\lambda = \Delta^{5/2} O\Big(\sum_{(p_1,q_1)} \sum_{(p_2,q_2)} n_{p_1}^{-1} n_{p_2}^{-1} \|v_{p_1q_1} v_{p_2q_2}^{*,T}\| \big(\sqrt{p_1} + \sqrt{q_1} + \sqrt{p_2} + \sqrt{q_2}\big)\Big). \tag{37}$$

From (30),

$$\|v_{pq}\|^2 = n_p \Delta^2 + O\big(\Delta^{5/2}(\sqrt{p} + \sqrt{|q|})\big).$$

Thus

$$\begin{aligned}\|v_{p_1q_1}v^{*,T}_{p_2q_2}\| &\leq \|v_{p_1q_1}\|\|v_{p_2q_2}\| \\ &= O\Big(\sqrt{n_{p_1}n_{p_2}}\Delta^2+\sqrt{n_{p_1}}\big(p_2^{1/4}+|q_2^{1/4}|\big)\Delta^{9/4} \\ &\quad +\sqrt{n_{p_2}}\big(p_1^{1/4}+|q_1^{1/4}|\big)\Delta^{9/4}+\big(p_1^{1/4}+|q_1^{1/4}|\big)\big(p_2^{1/4}+|q_2^{1/4}|\big)\Delta^{5/2}\Big).\end{aligned}$$

Using this bound in (37), after some tedious but straightforward algebra we obtain the formula

$$\begin{aligned}\lambda(\lambda-\Delta^2) &= \Delta^{5/2}O\Big(\Delta^2N^{11/2}+\Delta^{9/4}N^{25/4}+\Delta^{5/2}N^7\Big) \\ &= O\Big(\Delta^{9/2}N^{11/2}+\Delta^{19/4}N^{25/4}+\Delta^5N^7\Big). \qquad (38)\end{aligned}$$

By solving the quadratic equation, we get that

$$|\lambda| = \Delta^2 + O\big(\Delta^{9/4}N^{11/4}\big).$$

Since we have already shown that $Var\, S_{1,N} = O(\Delta^4N^2)$, Condition 3 of de Jong [11] is evaluated as follows:

$$\frac{|\lambda|}{\sqrt{Var\, S_{1,N}}} = \frac{1}{N} + O(\Delta^{1/4}N^{7/4}).$$

Since $\Delta N^7 \to 0$, and all estimates are uniform over the eigenvalues of M, this finishes the proof of the first part of Theorem 1.
Now let us consider the case of an alternative hypothesis, i.e. $f \neq rf$. Let us start with the non–stochastic term $S_{3,N}$ in (29). First note that

$$S_{3,N} = \sum_{(p,q)} n_p^{-1}\big|E\hat{A}(\bar{f})\big|^2.$$

Then by virtue of Lemma 2 with $f(x,y)$ replaced by $\bar{f}(x,y)$, we have

$$S_{3,N} = \|f-rf\|^2/4 + O\big(N\Delta^{3/2}+N^{3/2}\Delta^\gamma+N^{-(2s+1)}\big). \qquad (39)$$

Next let us evaluate the variance of $S_{2,N}$. Note first that

$$VarS_{2,N} = 4\sigma^2\sum_{(x_i,y_j)\in D}\Big(\sum_{(x_k,y_l)\in D}\bar{f}(x_k,y_l)m_{(ij),(kl)}\Big)^2.$$

By expanding the formula in brackets and recalling the definition of the matrix M we obtain that

$$VarS_{2,N} = 4\sigma^2\bar{f}^TM^2\bar{f}, \qquad (40)$$

where the vector $\bar{f}$ is defined by $\bar{f} = \big(\bar{f}(x_i,y_j)\big)_{(x_i,y_j)\in D}$. The proof of the first part of the theorem, see formula (38), reveals that

$$M^2 = \Delta^2M + O(\Delta^{9/2}N^{11/2}).$$

This and (40) gives

$$Var\, S_{2,N} = 4\sigma^2\Delta^2\bar{f}^TM\bar{f} + \bar{f}^T\bar{f}\,O\big(\Delta^{9/2}N^{11/2}\big).$$

Observing that $\bar{f}^TM\bar{f} = S_{3,N}$ and using (39) we obtain

$$Var\, S_{2,N} = \sigma^2\Delta^2\|f-rf\|^2 + O\big(N\Delta^{7/2}+N^{3/2}\Delta^{\gamma+2}+\Delta^2N^{-(2s+1)}\big) + \|\bar{f}\|^2O\big(\Delta^{9/2}N^{11/2}\big).$$

Hence $Var\, S_{2,N}$ is of order Δ^2, and $S_{2,N}$ dominates the quadratic term $S_{3,N}$. Furthermore the remainder terms in (39) are negligible, even after dividing by the standard deviation Δ. Finally, we check Lyapounov's condition. We shall show that

$$\frac{E\epsilon_{11}^4 \sum_{(x_k,y_l)\in D} \Big| \sum_{(x_i,y_j)\in D} \bar{f}(x_i,y_j) m_{(ij),(kl)} \Big|^4}{\big(Var\, S_{2,N}\big)^2} \to 0. \tag{41}$$

The interior sum in the denominator can be evaluated as follows (cf. [38])

$$\begin{aligned} \sum_{(x_i,y_j)\in D} \bar{f}(x_i,y_j) m_{(ij),(kl)} &= \sum_{(p,q)} w^*_{pq}(x_k,y_l)\, n_p^{-1} \sum_{(x_i,y_j)\in D} \bar{f}(x_i,y_j) w_{pq}(x_i,y_j) \\ &= \sum_{(p,q)} w^*_{pq}(x_k,y_l)\, n_p^{-1} \big(A_{pq}(\bar{f}) + O(\Delta^\gamma)\big). \end{aligned} \tag{42}$$

From the proof of Lemma 3 in [38],

$$|A_{pq}(\bar{f})| = O\Big(\frac{1}{(|q|+1)(p+1)\sqrt{p-|q|+1}}\Big).$$

Using this we estimate the numerator in (41) by

$$\sum_{(x_k,y_l)\in D} \Big| \sum_{(x_i,y_j)\in D} \bar{f}(x_i,y_j) m_{(ij),(kl)} \Big|^4 = O\big((N\log(N))^4\Delta^6 + \Delta^{8\gamma+6}N^{12}\big),$$

and since $Var\, S_{2,N}$ is of order Δ^2, (41) is $O((N\log(N))^4\Delta^2 + \Delta^{8\gamma+2}N^{12})$, which tends to zero since $N^{3/2}\Delta^{\gamma-1} \to 0$. This finishes the proof of the theorem.

□

References

[1] I. A. Ahmad and Q. Li, "Testing symmetry of an unknown density function by kernel method," *J. Nonparametr. Statist.*, vol. 7, pp. 279–293, 1997.

[2] A. Antille, G. Kersting, and W. Zucchini, "Testing symmetry," *J. American Statist. Assoc.*, vol. 77, pp. 639–646, 1982.

[3] M. J. Atallah, "On symmetry detection," *IEEE Trans. Comput.* vol. C–34, pp. 663–666, 1985.

[4] N. Bissantz, H. Holzmann, and M. Pawlak, "Testing for image symmetry - technical details," Technical Report, Ruhr-Universität Bochum, 2008.

[5] R. R. Bailey and M. Srinath, "Orthogonal moment feature for use with parametric and non-parametric classifiers," *IEEE Trans. Pattern Analysis and Machine Intelligence*, vol. 18, pp. 389–396, 1996.

[6] P. J. Bickel, "On adaptive estimation," *Ann. Statist.*, vol. 10, pp. 647–671, 1982.

[7] N. Bissantz, G. Claeskens, H. Holzmann, and A. Munk, "Testing for lack of fit in inverse regression – with applications to biophotonic imaging," *J. Roy. Statist. Soc. Ser. B*, to appear, 2008.

[8] M. Born and E. Wolf, "On the circle polynomials of Zernike and related orthogonal sets," *Proc. Cambridge Philos. Soc.*, vol. 50, pp. 40–48, 1954.

[9] J.H. Conway, H. Burgiel, and C. Goodman-Strauss, *The Symmetry of Things*. Wellesley, MA, A K Peters, 2008.

[10] S. Derrode and F. Ghorbel, "Shape analysis and symmetry detection in gray-level objects using the analytical Fourier-Mellin representation," *Signal Processing*, vol. 84, pp. 25-39, 2004.

[11] P. de Jong, "A central limit theorem for generalized quadratic forms," *Probab. Theory Related Fields*, vol. 75, pp. 261–277, 1987.

[12] H. Dette and A. Munk, " Validation of linear regression models," *Ann. Statist.*, vol. 26, pp. 778–800, 1998.

[13] H. Dette, "A consistent test for the functional form of a regression based on a difference of variance estimators," *Ann. Statist.*, vol. 27, pp. 1012–1040, 1999.

[14] H. Dette, S. Kusi-Appiah, and N. Neumeyer, "Testing symmetry in nonparametric regression models," *J. Nonparametr. Stat.*, vol. 14, pp. 477–494, 2002.

[15] I.L. Dryden and K.V. Mardia, *Statistical Shape Analysis*. New York, Wiley, 1998.

[16] Y. Fan and R. Gencay, "A consistent nonparametric test of symmetry in linear regression models,"*J. Amer. Statist. Assoc.*, vol. 90, pp. 551–557, 1995.

[17] S. A. Friedberg, "Finding axes of skewed symmetry", *Comput. Vision Graphics Image Process*, vol. 32, pp. 138–155, 1986.

[18] P. Hall, *The Bootstrap and Edgeworth Expansion*. Springer-Verlag, New York, 1992.

[19] W. Härdle and E. Mammen, "Comparing nonparametric versus parametric regression fits.," *Ann. Statist.*, vol. 21, pp.1926–1947, 1993.

[20] J. D. Hart, *Nonparametric Smoothing and Lack-of-Fit Tests*. Springer, New York, 1997.

[21] J. Horowitz and V. Spokoiny, "An adaptive, rate-optimal test of a parametric mean-regression model against a nonparametric alternative," *Econometrica*, vol. 69, pp. 599-631, 2001.

[22] J. C. Hsu, *Multiple Comparisions – Theory and Methods*. Chapman and Hall, London, 1996.

[23] D.R. Iskander, M. J. Collins, and B. Davis, "Optimal modeling of corneal surfaces with Zernike polynomials," *IEEE Trans. Biomedical Engineering*, vol. 48, pp. 87-95, 2001.

[24] Y. Keller and Y. Shkolnisky, "A signal processing approach to symmetry detection," *IEEE Trans. on Image Processing*, vol.15, pp.2198-2207, 2006.

[25] N. Kiryati and Y. Gofman, "Detecting symmetry in grey level images: the global optimisation approach," *Int. Journal of Computer Vision*, vol. 29, pp. 29-45, 1998.

[26] I. M. Johnstone and B. W. Silverman, "Speed of estimation in positron emission tomography and related inverse problems," *Ann. Statist.*, vol. 18, pp. 251–280, 1990.

[27] W.-Y. Kim and Y.-S. Kim, "Robust rotation angle estimator," *IEEE Trans. Pattern Analysis and Machine Intelligence*, vol 21, pp. 768–773, 1999.

[28] A. Khotanzad and Y. H. Hong, "Invariant image recognition by Zernike moments," *IEEE Trans. Pattern Anal. Machine Intell.*, vol. 12, pp. 489–498, 1990.

[29] J. Lehr, J.-B. Sibarita, and J.-M. Chassery, "Image restoration in X-ray microscopy: PSF determination and biological applications", *IEEE Trans. Image Processing*, vol. 7, pp. 258–263, 1998.

[30] F. Leblanc and O. V. Lepski, "Test of symmetry in nonparametric regression," *Theory Probab. Appl.*, vol. 47, pp. 34–52, 2003.

[31] S. X. Liao and M. Pawlak, "On image analysis by moments," *IEEE Trans. Pattern Analysis and Machine Intelligence*, vol. 18, pp. 254–266, 1996.

[32] S. X. Liao and M. Pawlak, "On the accuracy of Zernike moments for image analysis," *IEEE Trans. Pattern Analysis and Machine Intelligence*, vol. 20, pp. 1358–1364, 1998.

[33] L. Lucchese, "Frequency domain classification of cyclic and dihedral symmetries of finite 2-D patterns," *Pattern Recognition*, vol. 37, pp. 2263–2280, 2004.

[34] G. Marola, "On the detection of the axes of symmetry of symmetric and almost symmetric planar images," *IEEE Trans. Pattern Anal. Mach. Intell.*, vol. 11, pp. 104–108, 1989.

[35] R. Mukundan and K. Ramakrishnan, *Moment Functions in Image Analysis: Theory and Applications,* World Scientific, 1998.

[36] A. Munk, N. Bissantz, T. Wagner, and G. Freitag, "On difference-based variance estimation in nonparametric regression when the covariate is high dimensional," *J. R. Statist. Soc. B*, vol. 67, pp. 19–41, 2005.

[37] P. Pankajakshan, B. Zhang, L. Blanc-Féraud, Z. Kam, J.-C. Olivo-Marin, and J. Zerubia, "Blind deconvolution for diffraction-limited fluorescence microscopy", *IEEE International Symposium on Biomedical Imaging*, 2008.

[38] M. Pawlak and S. X. Liao, "On the recovery of a function on a circular domain," *IEEE Trans. Inform. Theory*, vol. 48, pp. 2736–2753, 2002.

[39] D. A. Pintsov, "Invariant pattern recognition, symmetry, and Radon transforms," *J. Opt. Soc. Am. A*, vol. 6, pp. 1544–1554, 1989.

[40] J. Rosen, *Symmetry in Science: An Introduction to the General Theory*. New York, Springer, 1995.

[41] O.D Trier, A.K. Jain, and T. Taxt, "Feature extraction methods for character recognition- A survey," *Pattern Recognition,* vol. 29, pp. 641-662, 1996.

[42] M. R. Teague, "Image analysis via the general theory of moments", *J. Opt. Soc. Am.*, vol. 70, pp. 920–930, 1980.

[43] A. V. Tuzikov, O. Colliot, and I. Bloch, "Evaluation of the symmetry plane in 3D MR brain images", *Pattern Recognition Letters*, vol. 24, pp. 2219–2233, 2003.

[44] Z. Xiao, Z. Hou, C. Miao, and J. Wang, "Using phase information for symmetry detection," *Pattern Recognition Lett.*, vol. 26, pp. 1985–1994, 2005.

[45] Y. Xin, M. Pawlak, and S. Liao, "Accurate computation of Zernike moments in polar coordinates," *IEEE Trans. on Image Processing*, vol.16, pp.581-587, 2007.

[46] F. Zernike, "Beugungstheorie des Schneidenverfahrens und seiner verbesserten Form, der Phasenkontrastmethode," *Physica*, vol. 1, pp. 689–701, 1934.